SCIENCE CHINA
Information Sciences

June 2023, Vol. 66 160408:1–160408:7
https://doi.org/10.1007/s11432-023-3758-4

• RESEARCH PAPER •
Special Topic: Two-Dimensional Materials and Device Applications

# Simultaneous optimization of phononic and electronic transport in two-dimensional $Bi_2O_2Se$ by defect engineering

Fang YANG[1], Hong Kuan NG[2], Jing WU[2], Yunshan ZHAO[3*] & Junpeng LU[1*]

[1]*School of Physics, Southeast University, Nanjing* 211189*, China;*
[2]*Institute of Materials Research and Engineering, Agency for Science, Technology and Research, Singapore* 138634*, Singapore;*
[3]*NNU-SULI Thermal Energy Research Center (NSTER) & Center for Quantum Transport and Thermal Energy Science (CQTES), School of Physics and Technology, Nanjing Normal University, Nanjing* 210023*, China*

Received 25 January 2023/Revised 18 March 2023/Accepted 5 May 2023/Published online 19 May 2023

**Abstract** Defect engineering represents one degree of freedom to tune the physical and chemical properties of two-dimensional (2D) materials. Here, we demonstrate that the thermal and electronic properties of 2D $Bi_2O_2Se$ can be optimized simultaneously by introducing oxygen defects. 2D $Bi_2O_2Se$ and its oxygen-deficient counterpart ($Bi_2O_xSe$, $x < 2$) can be controllably synthesized by the chemical vapor deposition (CVD) method. By introducing oxygen defects, the thermal conductivity of 2D $Bi_2O_2Se$ is reduced by nearly three times, achieving an extremely low thermal conductivity of $0.68 \pm 0.06$ W/mK at room temperature via the thermal bridge technique. This low thermal conductivity is enabled by the scattering of phonons by targeting of high-, mid-, and low-frequency phonons due to oxygen defects, strong anharmonicity, and nanostructure boundaries, respectively. Meanwhile, the mobility is also improved to 260–500 $cm^2 \cdot V^{-1} \cdot s^{-1}$ and the usual polar optical phonon scattering in 2D $Bi_2O_2Se$ is weakened owing to the introduction of oxygen defects. Our results promise potential applications for thermoelectric design, nanoelectronics, and thermal barrier coating devices based on emerging 2D materials.

**Keywords** 2D $Bi_2O_2Se$, thermal conductivity, oxygens defects, phonon scattering, mobility

**Citation** Yang F, Ng H K, Wu J, et al. Simultaneous optimization of phononic and electronic transport in two-dimensional $Bi_2O_2Se$ by defect engineering. Sci China Inf Sci, 2023, 66(6): 160408, https://doi.org/10.1007/s11432-023-3758-4

## 1 Introduction

The emergence of two-dimensional (2D) materials, such as graphene and transition-metal dichalcogenides (TMDs), has attracted broad interest in many research fields [1, 2]. The unique van der Waals stacking of 2D materials breaks the limitation of traditional bulk materials and opens up numerous competitive applications in electronics, optoelectronics, and thermoelectrics [3–5]. However, in these applications, performance is constrained by their thermal properties, which directly affect the heat dissipation in electronic devices and energy conversion efficiency in thermoelectric devices [6]. For example, on the one hand, the high thermal conductivity of graphene (≈5000 W/mK) and h-BN (≈800 W/mK) is beneficial for alleviating the issue of Joule heating [7, 8]. On the other hand, low thermal conductivity is also essential for thermal barrier coatings and for thermoelectrics to maintain high temperature gradients to achieve high efficiency [9, 10]. To this end, effective methods to tune the phonon transport and thermal properties in 2D materials are crucial.

Many strategies have been formulated to suppress thermal conductivity, such as resonant scattering by localized rattling atoms, interface scattering by reducing grain size, artificial superlattices, isotope engineering, and defect engineering [11, 12]. Among these, defect engineering is almost always the most

* Corresponding author (email: phyzys@njnu.edu.cn, phyljp@seu.edu.cn)

 

effective way to regulate phonon transport and thermal conductivity, which could largely decrease the total relation time of phonons over a broad range of phonon frequencies [12–16]. As reported in many recent studies, the alteration of phonon transport by defect engineering has been widely demonstrated in 2D materials. For example, the thermal conductivity of graphene can be reduced by 90% by introducing defects with oxygen plasma treatment [14]. In transition metal dichalcogenides (TMDCs), Zhao et al. [15] proved that helium ion ($He^+$) irradiation-induced Mo vacancies greatly impede phonon transport and result in a large reduction of 80% in thermal conductivity. Aiyiti et al. [16] demonstrated that the phonon transmission coefficient of the defective $MoS_2$ can be decreased significantly for nearly the entire phonon frequency range. Among numerous 2D materials, $Bi_2O_2Se$ has attracted extensive attention owing to its high carrier mobility, moderate band gap, excellent mechanical properties, and outstanding stability in the ambient environment [17, 18]. Compared with graphene, 2D TMDs, and other 2D materials, the intrinsic low group velocity and strong anharmonic phonon scattering make $Bi_2O_2Se$ a promising material for applications in thermoelectrics and thermal barrier coatings [19, 20]. Although defect regulation in 2D $Bi_2O_2Se$ has shown good effects in tuning electronic and optoelectronic properties, a direct experimental demonstration of defect regulation in phonon transport and thermal conductivity of 2D $Bi_2O_2Se$ is still lacking [21, 22].

In this work, we experimentally probed the effect of oxygen defects on the thermal transport in $Bi_2O_2Se$ by employing the traditional thermal bridge method. We found that the thermal conductivity of $Bi_2O_xSe$ can be significantly reduced by introducing oxygen vacancies and that the room-temperature thermal conductivity reaches as low as $0.68 \pm 0.06$ W/mK, which is nearly three times lower than $Bi_2O_2Se$ (1.2–1.9 W/mK in our experiment). Furthermore, $Bi_2O_xSe$ shows relatively weak temperature-dependent thermal conductivities compared with $Bi_2O_2Se$ due to dominant defect-phonon scattering. Unlike the usual defect-induced phonon scattering that decreases both the electrical conductivity and carrier mobility, the carrier mobility of $Bi_2O_xSe$ is observed to significantly increase. To elucidate the scattering physics, we measured the temperature-dependent electric transport of both $Bi_2O_xSe$ and $Bi_2O_2Se$. By introducing oxygen defects, the dominant scattering mechanism changes from polar optical phonon scattering (POP) in $Bi_2O_2Se$ to acoustic phonon scattering (AP) in $Bi_2O_xSe$, leading to room-temperature carrier mobility ranging between 260–500 $cm^2 \cdot V^{-1} \cdot s^{-1}$.

## 2 Results and discussion

As shown in Figure 1(a), $Bi_2O_2Se$ has a tetragonal structure with I4/mmm ($a = b = 3.88$ Å, $c = 12.16$ Å) space symmetry group, where $[Bi_2O_2]_n$ layers and $[Se]_n$ layers are combined with weak electrostatic interactions [17]. Figure 1(b) shows an optical image of few-layer $Bi_2O_2Se$ with 20–30 μm domain size grown using the low-pressure chemical vapor deposition (CVD) method. The AFM image exhibits a uniform surface with a thickness of 10.1 nm. In addition to the square flakes, right-angled triangular flakes are also observed in the grown $Bi_2O_2Se$ samples, as shown in Figure 1(c). As previously reported by Li et al. [23], such triangular flakes originate from a different growth kinetic process owing to O deficiencies, which then result in nonstoichiometric $Bi_2O_xSe$. At high growth temperatures, the high migration of adatoms leads to a thermodynamically stable growth process, which produces stoichiometric $Bi_2O_2Se$ flakes. At low growth temperatures, triangular $Bi_2O_2Se$ tends to grow in the vertical direction along the (110) plane to lower the system energy, and the absence of oxygen atoms makes the growth process thermodynamically unstable, resulting in nonstoichiometric $Bi_2O_xSe$ flakes. And the proportion of the square and triangle samples can be controlled by tuning the growth temperature. The detailed CVD growth progress can be found in Figure S1. The Raman spectra comparing $Bi_2O_2Se$ and $Bi_2O_xSe$ measured are shown in Figure 1(d), where a prominent $A_{1g}$ Raman mode at approximately 158.2 $cm^{-1}$ is observed in $Bi_2O_2Se$ arising from the Bi-O layer [24]. For $Bi_2O_xSe$, the $A_{1g}$ Raman peak shows an obvious redshift to approximately 161.36 $cm^{-1}$ [25]. This redshift originates from reduced phonon vibration due to the introduction of oxygen atom vacancies, which indicates a decrease in lattice thermal conductivity.

To investigate the bonding strength after introducing oxygen defects, we characterized $Bi_2O_2Se$ and $Bi_2O_xSe$ using X-ray photoelectron spectroscopy (XPS), which is sensitive to chemical bonds (Figures 1(e) and S2). In $Bi_2O_2Se$, two symmetric peaks of Bi $4f_{7/2}$ and Bi $4f_{5/2}$ were centered at 163.94 and 158.65 eV, respectively, which is consistent with [26]. In $Bi_2O_xSe$, the Bi $4f_{7/2}$ and Bi $4f_{5/2}$ peaks were measured at 163.5 and 158.2 eV, respectively. Here, the lower binding energy observed is attributed to the increase in the outer shell electron density of Bi and the increased shielding effect of the outer shell electrons on the

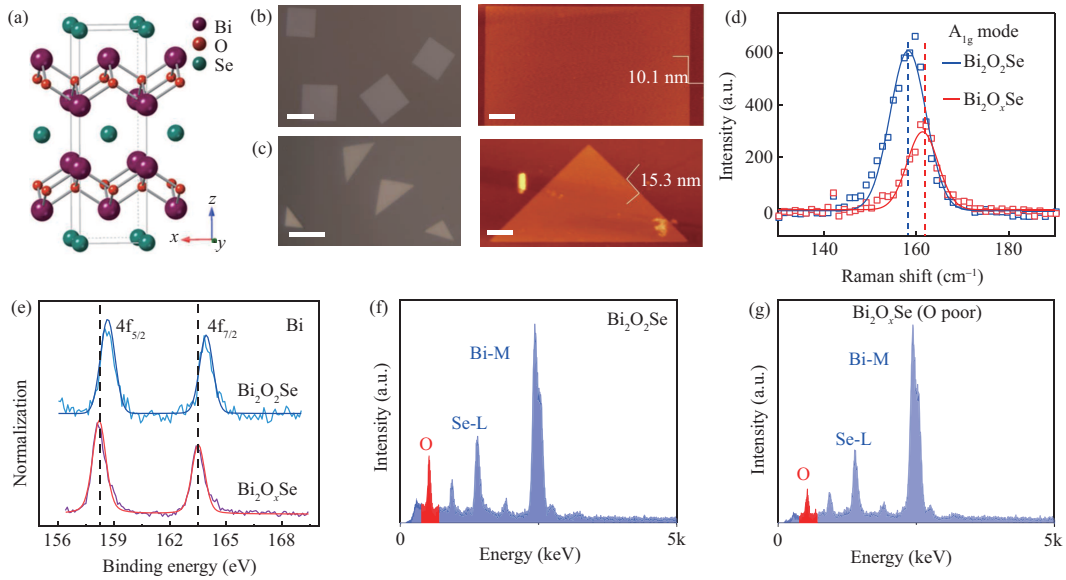


**Figure 1** (Color online) Characterization of $Bi_2O_2Se$ and $Bi_2O_xSe$ flakes. (a) Crystal structure of $Bi_2O_2Se$; (b) optical (scale bar: 10 μm) and AFM images (scale bar: 2 μm) of the as-grown square $Bi_2O_2Se$ flake; (c) optical (scale bar: 20 μm) and AFM images (scale bar: 3 μm) of the as-grown triangular $Bi_2O_xSe$ flake; (d) Raman spectroscopy of the $A_{1g}$ vibration mode of $Bi_2O_2Se$ and $Bi_2O_xSe$; (e) Bi 4f spectra of $Bi_2O_2Se$ and $Bi_2O_xSe$ with Gaussian fitting; (f) and (g) EDS spectrum in TEM of $Bi_2O_2Se$ and $Bi_2O_xSe$ nanosheets.

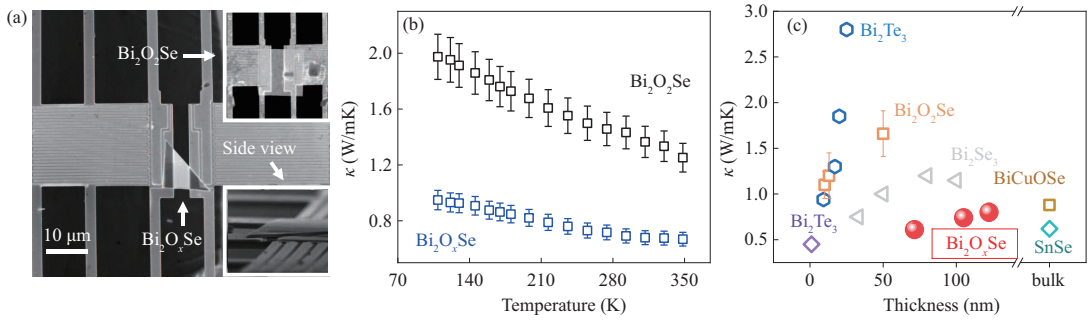


**Figure 2** (Color online) Thermal transport of $Bi_2O_2Se$ and $Bi_2O_xSe$. (a) Thermal bridge of the transferred $Bi_2O_xSe$ flake and $Bi_2O_2Se$ flake; (b) temperature-dependent thermal conductivity of $Bi_2O_2Se$ and $Bi_2O_xSe$; (c) thickness-dependent thermal conductivity of $Bi_2O_2Se$ and $Bi_2O_xSe$ compared with other thermoelectric materials: $Bi_2Se_3$, $Bi_2Te_3$, BiCuOSe, and SnSe.

inner shell electrons due to the oxygen defects. As a result, the bonding energy decreased, and an obvious shift was observed. Figures 1(f) and (g) show the energy dispersive spectrometer (EDS) for transmission electron microscopy (TEM) characterization, where the reduction in oxygen content in $Bi_2O_xSe$ can be clearly seen, while the Bi and Se atoms remain almost unchanged. The EDS spectrum mapping (Bi, O, Se) in TEM of $Bi_2O_2Se$ and $Bi_2O_xSe$ is in Figures S3–S5.

To investigate the thermal transport of $Bi_2O_2Se$ and $Bi_2O_xSe$, a suspended microelectron-thermal system (METS) was employed, which was fabricated following a process similar to a previous report by Shi et al. [27]. A 300-nm-thick $SiN_x$ layer was used as mechanical support, and top Pt metallization of 60 nm was used as electrodes. The sensor and heater contained a Pt loop as the resistance thermometer suspended by six long beams for thermal isolation from the substrate bulk. For thermal isolation from the substrate, both the sensor and heater were suspended using six long beams. The $Bi_2O_2Se$ and $Bi_2O_xSe$ flakes were then transferred onto METS using a poly(methyl methacrylate) (PMMA)-mediated method and thereafter loaded into a cryostat for thermal measurements (Figure 2(a)). A direct current (DC), $I_h$, was applied across the heater loop to generate a temperature gradient via Joule heating. The four-terminal resistance loop of heater $R_h$ and sensor $R_s$ were acquired by the lock-in amplifiers. The heater temperature $T_h$ and sensor temperature $T_s$ were obtained based on $R_h$ and $R_s$, which have been calibrated previously. Based on the equivalent thermal circuit, the thermal conductance ($G$) and thermal

conductivity ($\kappa$) can be calculated as [27]

$$G = G_{\rm b}\frac{\Delta T_{\rm s}}{\Delta T_{\rm h} - \Delta T_{\rm s}} = \frac{(R_{\rm h}{+}1/2R_{\rm b})I_{\rm h}^2\Delta T_{\rm s}}{\Delta T_{\rm h}^2 - \Delta T_{\rm s}^2},$$

$$\kappa = GL/A,$$

where $R_{\rm b}$ is the electrical resistance of each connecting beam passing the heating current $I_{\rm h}$. $\Delta T_{\rm h}, \Delta T_{\rm s}$ are the temperature rise of the heater and sensor, respectively. $L, A$ are the length and cross-sectional area of the suspended sample. The contact thermal resistance is analyzed by the fin thermal resistance model [28]. Figure 2(b) shows a distinct difference in thermal conductivity between $Bi_2O_2Se$ and $Bi_2O_xSe$. For a 50.1-nm-thick $Bi_2O_2Se$ flake, the thermal conductivity is 1.71 ± 0.25 W/mK, which is consistent with first-principles calculations and micro-Raman photothermal measurements [19, 29]. For a 71.4-nm-thick $Bi_2O_xSe$ flake, the thermal conductivity reaches as low as 0.68 ± 0.06 W/mK, which is lower than that of most two-dimensional materials [5]. This reduction in thermal conductivity can be explained by phonon group velocity and phonon scattering. In $Bi_2O_2Se$, Bi and O atoms are bound together due to strong covalent interactions, and the weak electrostatic interactions of the Bi-O layer with the Se layer are responsible for the low phonon velocity. In $Bi_2O_xSe$, the XPS result reveals a significantly weakened bonding energy of the Bi atom, which leads to a much lower phonon velocity and lowers thermal conductivity. Moreover, due to the absence of O atoms, the localized vibration of adjacent Bi atoms constitutes additional lying low-frequency optical phonon modes [30]. These low-frequency optical phonon modes coupled with acoustic phonons and consequently suppress the phonon mean free path, leading to low thermal conductivity. Next, we consider phonon scattering in $Bi_2O_xSe$. The interlayer interaction of Bi and Se atoms causes intrinsically strong anharmonic scattering [31]. By introducing O vacancies, the undercoordinated Bi atoms largely scatter high-frequency phonons. With a combination of nanostructure boundaries to target low-frequency phonons and inherent anharmonicity to target mid-frequency phonons, full-spectrum phonon scattering is achieved to enable the extremely low thermal conductivity in 2D $Bi_2O_2Se$. Figure 2(b) shows the temperature-dependent thermal conductivity for $Bi_2O_2Se$ and $Bi_2O_xSe$. Compared with $Bi_2O_2Se$, $Bi_2O_xSe$ shows a relatively temperature-insensitive thermal conductivity. In $Bi_2O_2Se$, phonon transport is dominated by intrinsic Umklapp scattering. As the temperature decreases, this Umklapp scattering is weakened, and the thermal conductivity is increased. For $Bi_2O_xSe$, phonon transport is instead dominated by phonon-defect scattering and is relatively insensitive to changes in temperature. The thickness-dependent thermal conductivities of $Bi_2O_2Se$ and $Bi_2O_xSe$ are further investigated. From Figure 2(c), the thermal conductivity gradually decreases with decreasing thickness, which can be attributed to the increased phonon boundary scattering rate [29]. Furthermore, we compared the thermal conductivity of $Bi_2O_xSe$, $Bi_2O_2Se$ with thermoelectric materials: $Bi_2Se_3$, $Bi_2Te_3$, BiCuOSe, and SnSe [32–36]. The low thermal conductivity makes $Bi_2O_xSe$ a material with great potential in the application of thermoelectrics and thermal barrier coatings.

While defects lead to a sharp decrease in thermal conductivity, the induced strong phonon scattering often leads to a decrease in carrier mobility, which is undesirable for thermoelectric and electronic devices. To investigate the electrical properties, we transferred $Bi_2O_2Se$ and $Bi_2O_xSe$ nanoplates from mica to a 285 nm $Si/SiO_2$ substrate with a PMMA-mediated method and fabricated back-gated field-electric transistors. Surprisingly, $Bi_2O_xSe$ exhibited an even higher electric conductivity and mobility than $Bi_2O_2Se$ (Figures 3(a) and S6), with mobility values of $Bi_2O_xSe$ reaching 260–500 $\rm cm^2{\cdot}V^{-1}{\cdot}s^{-1}$ at room temperature, in agreement with [37, 38]. The mobility is extracted from transfer characteristics, via $\mu = \frac{1}{C_{ox}}\frac{L}{W}\frac{{\rm d}G}{{\rm d}V_g}$, where $C_{ox}$ is the capacitance of $SiO_2$ and $L, W$ are length, width of the device, respectively (Figure 3(b)). To better understand the underlying mechanism for the observed mobility enhancement, cryogenic measurements (77–300 K) of $Bi_2O_2Se$ and $Bi_2O_xSe$ were performed. Obvious metallic behavior was observed in both $Bi_2O_2Se$ and $Bi_2O_xSe$, as shown in Figure 3(c). With increasing temperature (especially over 160 K), a sharp decrease in mobility in $Bi_2O_2Se$ was observed, which is consistent with previous reports (Figure 3(d)) [20]. Compared with $Bi_2O_2Se$, the mobility in $Bi_2O_xSe$ decays more slowly with decreasing temperature. The temperature dependence of electron mobility can be described by the formula $\mu \sim T^{-\lambda}$. For $Bi_2O_2Se$, the value of $\lambda$ reaches 4.0, which indicates dominant polar-optical phonon scattering [39]. In the $Bi_2O_2Se$ phonon spectrum, the acoustic branches and low-frequency optical branches are mainly contributed by Bi and Se atoms, and high-frequency optical branches are dominated by O atoms according to the first-principal calculation [29]. Although the high-frequency

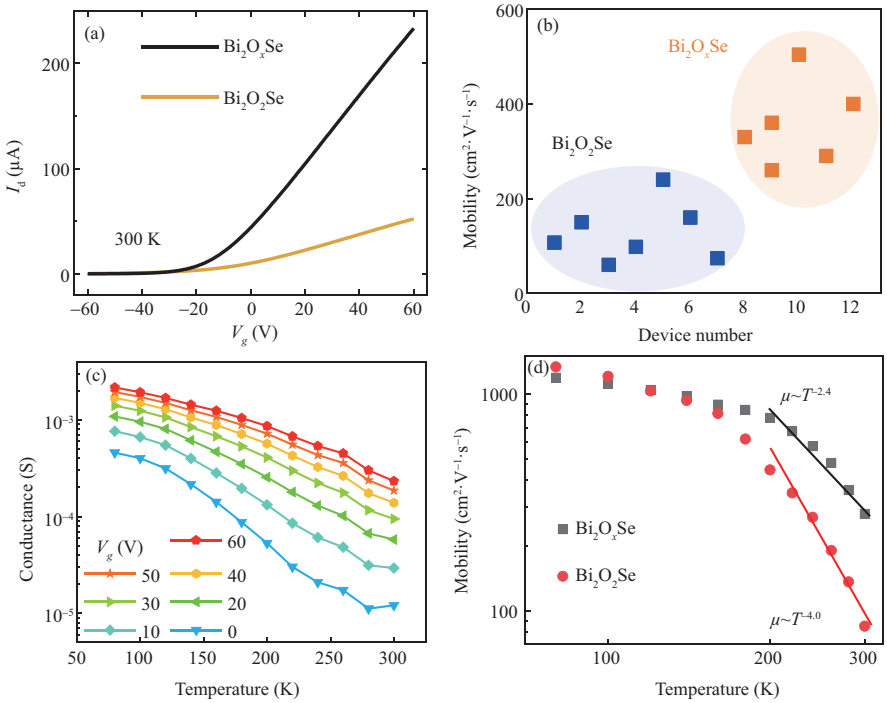


**Figure 3** (Color online) Electronic transport of $Bi_2O_2Se$ and $Bi_2O_xSe$. (a) $I_d$-$V_g$ transfer curves of $Bi_2O_2Se$ and $Bi_2O_xSe$ at room temperature; (b) comparison of room temperature carrier mobility of multi $Bi_2O_2Se$- and $Bi_2O_xSe$-based devices; (c) temperature dependence of the conductance of $Bi_2O_xSe$ and $Bi_2O_2Se$; (d) temperature dependence of the mobility of $Bi_2O_xSe$ and $Bi_2O_2Se$.

optical branches dominated by O atoms have little impact on heat transfer, they dominate electron scattering at high temperatures [29]. Moreover, Liu et al. [40] revealed the fine structure distortion in $Bi_2O_2Se$ by polarization-dependent third-harmonic generation (THG). The rotation of O atoms ($\leqslant 1.4°$) in Bi-O layers breaks the symmetry and leads to the transition from the $D_{4h}$ to $C_{4h}$ point group, which results in the polar nature of $Bi_2O_2Se$.

Thus, polar-optical phonon scattering becomes dominant, and strong electron-phonon scattering leads to a sharp decrease in mobility at high temperatures. For $Bi_2O_xSe$, the value is reduced to 2.4, which indicates that both optical and acoustical phonon scattering become dominant. Although oxygen vacancies cause a large amount of undercoordinated Bi atoms and lead to stronger acoustic-phonon scattering, optical-phonon scattering is the main factor that limits its intrinsic high mobility at room temperature. The vacancy of O atoms results in the absence of some optical branches and weakens the polar-optical phonon scattering. As a result, the mobility in $Bi_2O_xSe$ shows a weak temperature dependence and increases significantly at room temperature. This demonstrates the multiple functionalities of defects in $Bi_2O_2Se$ acting beneficially as weakening optical-phonon scattering to decrease electron-phonon scattering for high mobility and blocking the acoustic phonon to suppress heat transport. The two key parameters, thermal conductivity and electric conductivity, can be effectively decoupled by defect engineering and modifying them toward higher thermoelectric properties in $Bi_2O_2Se$. These results provide a new strategy for simultaneously lowering the thermal conductivity and improving the carrier mobility in oxide thermoelectric materials, which is the prime task for realizing high-performance thermoelectrics.

## 3 Conclusion

In summary, we demonstrated that defect engineering can enormously affect several key properties in $Bi_2O_2Se$ and $Bi_2O_xSe$ using tunable chemical vapor deposition growth $Bi_2O_2Se$ and $Bi_2O_xSe$. Using thermal bridge measurements, we revealed that oxygen defects in $Bi_2O_2Se$ can lead to a nearly three-fold reduction in thermal conductivity. In addition to the strong anharmonic scattering-induced intrinsic low thermal conductivity of 2D $Bi_2O_xSe$, oxygen defects introduce additional strong phonon-defect scattering and result in an ultralow room temperature thermal conductivity of $0.68 \pm 0.06$ W/mK. Moreover, an enhancement of electric conductivity and carrier mobility in $Bi_2O_xSe$ at room temperature is observed owing

to the switching of the dominant scattering mechanism from polar optical phonon scattering to acoustic phonon scattering. Overall, our results demonstrated the effectiveness of defect engineering in tuning the thermal properties and electronic properties of 2D materials, which is important for thermal management to achieve better performing thermoelectrics and nanoelectronics. Defect engineering provides a promising strategy for the development of 2D electronics, thermoelectrics, and quantum information sciences.

**Acknowledgements** This work was supported by National Key Research and Development Program of China (Grant Nos. 2019YFA0208000, 2021YFA1200700) and National Natural Science Foundation of China (Grant Nos. 62174026, 91963130).

**Supporting information** Figures S1–S6. The supporting information is available online at info.scichina.com and link.springer.com. The supporting materials are published as submitted, without typesetting or editing. The responsibility for scientific accuracy and content remains entirely with the authors.

**References**

1 Chang C, Chen W, Chen Y, et al. Recent progress on two-dimensional materials. Acta Physico Chim Sin, 2021, 37: 2108017
2 Akinwande D, Huyghebaert C, Wang C H, et al. Graphene and two-dimensional materials for silicon technology. Nature, 2019, 573: 507–518
3 Chhowalla M, Jena D, Zhang H. Two-dimensional semiconductors for transistors. Nat Rev Mater, 2016, 1: 1–5
4 Li X, Tao L, Chen Z, et al. Graphene and related two-dimensional materials: structure-property relationships for electronics and optoelectronics. Appl Phys Rev, 2017, 4: 021306
5 Zhou Y, Zhao L D. Promising thermoelectric bulk materials with 2D structures. Adv Mater, 2017, 29: 1702676
6 Ong Z Y, Bae M H. Energy dissipation in van der Waals 2D devices. 2D Mater, 2019, 6: 032005
7 Balandin A A, Ghosh S, Bao W, et al. Superior thermal conductivity of single-layer graphene. Nano Lett, 2018, 8: 902–907
8 Cai Q, Scullion D, Gan W, et al. High thermal conductivity of high-quality monolayer boron nitride and its thermal expansion. Sci Adv, 2019, 5: eaav0129
9 Zhao L D, Tan G, Hao S, et al. Ultrahigh power factor and thermoelectric performance in hole-doped single-crystal SnSe. Science, 2016, 351: 141–144
10 Miller R A. Current status of thermal barrier coatings—an overview. Surf Coatings Tech, 1987, 30: 1–11
11 Wan C, Wang Y, Wang N, et al. Development of novel thermoelectric materials by reduction of lattice thermal conductivity. Sci Tech Adv Mater, 2010, 11: 044306
12 Savin A V, Kivshar Y S, Hu B. Suppression of thermal conductivity in graphene nanoribbons with rough edges. Phys Rev B, 2010, 82: 195422
13 Zhao Y, Liu D, Chen J, et al. Engineering the thermal conductivity along an individual silicon nanowire by selective helium ion irradiation. Nat Commun, 2017, 8: 15919
14 Zhao W, Wang Y, Wu Z, et al. Defect-engineered heat transport in graphene: a route to high efficient thermal rectification. Sci Rep, 2015, 5: 11962
15 Zhao Y, Zheng M, Wu J, et al. Modification of thermal transport in few-layer $MoS_2$ by atomic-level defect engineering. Nanoscale, 2021, 13: 11561–11567
16 Aiyiti A, Hu S, Wang C, et al. Thermal conductivity of suspended few-layer $MoS_2$. Nanoscale, 2018, 10: 2727–2734
17 Wu J, Yuan H, Meng M, et al. High electron mobility and quantum oscillations in non-encapsulated ultrathin semiconducting $Bi_2O_2Se$. Nat Nanotech, 2017, 12: 530–534
18 Li T, Peng H. 2D $Bi_2O_2Se$: an emerging material platform for the next-generation electronic industry. Acc Mater Res, 2021, 2: 842–853
19 Yang F, Wang R, Zhao W, et al. Thermal transport and energy dissipation in two-dimensional $Bi_2O_2Se$. Appl Phys Lett, 2019, 115: 193103
20 Yang F, Wu J, Suwardi A, et al. Gate-tunable polar optical phonon to piezoelectric scattering in few-layer $Bi_2O_2Se$ for high-performance thermoelectrics. Adv Mater, 2021, 33: 2004786
21 Luo H, Gao Q, Liu H, et al. Electronic nature of charge density wave and electron-phonon coupling in kagome superconductor $KV_3Sb_5$. Nat Commun, 2022, 13: 273
22 Dang L Y, Liu M, Wang G G, et al. Organic ion template-guided solution growth of ultrathin bismuth oxyselenide with tunable electronic properties for optoelectronic applications. Adv Funct Mater, 2022, 32: 2201020
23 Li J, Wang Z, Wen Y, et al. High-performance near-infrared photodetector based on ultrathin $Bi_2O_2Se$ nanosheets. Adv Funct Mater, 2018, 28: 1706437
24 Cheng T, Tan C, Zhang S, et al. Raman spectra and strain effects in bismuth oxychalcogenides. J Phys Chem C, 2018, 122: 19970–19980
25 Hossain M T, Das M, Ghosh J, et al. Understanding the interfacial charge transfer in the CVD grown $Bi_2O_2Se/CsPbBr_3$ nanocrystal heterostructure and its exploitation in superior photodetection: experiment vs. theory. Nanoscale, 2021, 13: 14945–14959
26 Chen W, Khan U, Feng S, et al. High-fidelity transfer of 2D $Bi_2O_2Se$ and its mechanical properties. Adv Funct Mater, 2020, 30: 2004960
27 Shi L, Li D, Yu C, et al. Measuring thermal and thermoelectric properties of one-dimensional nanostructures using a microfabricated device. J Heat Transfer, 2003, 125: 881–888
28 Yang X, Zheng X, Liu Q, et al. Experimental study on thermal conductivity and rectification in suspended monolayer $MoS_2$. ACS Appl Mater Inter, 2020, 12: 28306–28312
29 Wang C, Ding G, Wu X, et al. Electron and phonon transport properties of layered $Bi_2O_2Se$ and $Bi_2O_2Te$ from first-principles calculations. New J Phys, 2018, 20: 123014
30 Samanta M, Pal K, Pal P, et al. Localized vibrations of Bi bilayer leading to ultralow lattice thermal conductivity and high thermoelectric performance in weak topological insulator n-type BiSe. J Am Chem Soc, 2018, 140: 5866–5872
31 Guo R, Jiang P, Tu T, et al. Electrostatic interaction determines thermal conductivity anisotropy of $Bi_2O_2Se$. Cell Rep Phys Sci, 2021, 2: 100624
32 Sun Y, Cheng H, Gao S, et al. Atomically thick bismuth selenide freestanding single layers achieving enhanced thermoelectric energy harvesting. J Am Chem Soc, 2012, 134: 20294–20297

33 Pettes M T, Maassen J, Jo I, et al. Effects of surface band bending and scattering on thermoelectric transport in suspended bismuth telluride nanoplates. Nano Lett, 2013, 13: 5316–5322

34 Sun G L, Li L L, Qin X Y, et al. Enhanced thermoelectric performance of nanostructured topological insulator $Bi_2Se_3$. Appl Phys Lett, 2015, 106: 053102

35 Zhao L D, Lo S H, Zhang Y, et al. Ultralow thermal conductivity and high thermoelectric figure of merit in SnSe crystals. Nature, 2014, 508: 373–377

36 Pei Y L, He J, Li J F, et al. High thermoelectric performance of oxyselenides: intrinsically low thermal conductivity of Ca-doped BiCuSeO. NPG Asia Mater, 2013, 5: e47

37 Tong T, Chen Y, Qin S, et al. Sensitive and ultrabroadband phototransistor based on two-dimensional $Bi_2O_2Se$ nanosheets. Adv Funct Mater, 2019, 29: 1905806

38 Li P, Han A, Zhang C, et al. Mobility-fluctuation-controlled linear positive magnetoresistance in 2D semiconductor $Bi_2O_2Se$ nanoplates. ACS Nano, 2020, 14: 11319–11326

39 Gelmont B L, Shur M, Stroscio M. Polar optical-phonon scattering in three- and two-dimensional electron gases. J Appl Phys, 1995, 77: 657–660

40 Liang J, Tu T, Chen G, et al. Unveiling the fine structural distortion of atomically thin $Bi_2O_2Se$ by third-harmonic generation. Adv Mater, 2020, 32: 2002831